*SMAI-JCM*
SMAI Journal of
Computational Mathematics

# A class of robust numerical schemes to compute front propagation

Nicolas Therme

Volume 4 (2018), p. 375-397.
<http://smai-jcm.cedram.org/item?id=SMAI-JCM_2018__4__375_0>

*SMAI Journal of Computational Mathematics*
Vol. 4, 375-397 (2018)

# A class of robust numerical schemes to compute front propagation

Nicolas Therme [1]

[1] Université de Nantes, Laboratoire de Mathématiques Jean Leray, CNRS UMR 6629, 2 rue de la Houssinière, BP 92208, 44322 Nantes, France
*E-mail address*: nicolas.therme@cea.fr.

**Abstract.** In this work a class of finite volume schemes is proposed to numerically solve equations involving propagating fronts. They fall into the class of Hamilton-Jacobi equations. Finite volume schemes based on staggered grids and initially developed to compute fluid flows, are adapted to the G-equation, using the Hamilton-Jacobi theoretical framework. The designed scheme has a maximum principle property and is consistent and monotonous on Cartesian grids. A convergence property is then obtained for the scheme on Cartesian grids and numerical experiments evidence the convergence of the scheme on more general meshes.

**2010 Mathematics Subject Classification.** 35F21, 65N08, 65N12.

**Keywords.** Finite volumes, Hamilton-Jacobi, Stability, Convergence.

## 1. Introduction

The work presented here falls into a larger thematic undertaken for several years, which is the development of numerical methods to simulate all Mach flow regimes [19, 7, 12, 27]. More precisely, the proposed numerical method enters the framework of staggered discretizations, mainly developed by J.C. Latché and R. Herbin. They derived from the classical Marker-And-Cell (MAC) scheme [18] and the seminal papers [16, 17], stating that this discretization is suitable for both compressible and incompressible flow problems. The use of staggered schemes in the incompressible case is now standard and the underlying convergence theory is well-known. Finite volume schemes were proposed for the compressible Navier-Stokes equations [15] and Euler equations [20, 21]. Adaptations of these schemes to more complex models, such as reactive mixture flows, is underway. In this context, equations describing reactive front propagation are involved and need to be discretized using natural extensions of the staggered schemes.

We focus on a particular equation, used in combustion science to simulate flame front propagation, the so called G-equation, which reads:

$$\partial_t(\rho G) + \operatorname{div}(\rho \boldsymbol{u} G) + \rho u_f |\boldsymbol{\nabla} G| = 0, \tag{1.1}$$

where $\rho$ is the density of the fluid, $G$ stands for the front indicator, $\boldsymbol{u}$ is a convective velocity and $u_f$ is a front propagation speed. The challenging issue is to adapt staggered discretizations to the last term $\rho u_f|\boldsymbol{\nabla} G|$ as the convective part of the equation has already been handled, in [15] for example. When combined with the mass balance equation of the system,

$$\partial_t \rho + \operatorname{div}(\rho \boldsymbol{u}) = 0,$$

the convective part of the equation is a transport operator and we get:

$$\partial_t G + \boldsymbol{u} \cdot \boldsymbol{\nabla} G + u_f |\boldsymbol{\nabla} G| = 0, \tag{1.2}$$

provided that the density never vanishes. This is a particular Hamilton-Jacobi equation. The theory of such equations is well known and was vastly developed by P.-L. Lions in [9, 24]. More precisely, consider the following Cauchy problem:

$$\begin{cases} \partial_t G + H(\boldsymbol{\nabla} G) = 0, \\ G(0, \boldsymbol{x}) = G_0(\boldsymbol{x}), \end{cases} \tag{1.3}$$

defined on $[0,T]\times\mathbb{R}^d$, with $H\in C(\mathbb{R}^d)$ and $G_0\in \mathrm{BUC}(\mathbb{R}^d)$, where $\mathrm{BUC}(\Omega)$ stands for the set of bounded uniformly continuous functions on $\Omega$. There exists exactly one solution $G\in \mathrm{BUC}([0,T]\times\mathbb{R}^d)$, such that $G(0,\boldsymbol{x})=G_0(\boldsymbol{x})$ and $G$ satisfies:

$$\begin{cases}\forall\phi\in C^1(\mathbb{R}^d\times(0,\infty)),\ \text{if } (x_0;t_0)\\ \text{is a local maximum of } G-\phi \text{ on } \mathbb{R}^d\times(0,T],\ \text{then},\\ \partial_t\phi(x_0,t_0)+H(\boldsymbol{\nabla}\phi(x_0,t_0))\leq 0\end{cases}\tag{1.4}$$

and

$$\begin{cases}\forall\phi\in C^1(\mathbb{R}^d\times(0,\infty)),\ \text{if } (x_0;t_0)\\ \text{is a local minimum of } G-\phi \text{ on } \mathbb{R}^d\times(0,T],\ \text{then},\\ \partial_t\phi(x_0,t_0)+H(\boldsymbol{\nabla}\phi(x_0,t_0))\geq 0.\end{cases}\tag{1.5}$$

We refer to [24] for more details. Various numerical methods exist to approach such viscosity solutions. A first converging finite difference scheme was developed in [10]. From this point high order extensions to this scheme were given by S. Osher and J. A. Sethian in [25] and a simple finite volume scheme was derived in [23], inspired from an unstructured finite difference scheme based on triangular meshes developed by R. Abgrall in [1]. The convergence theory of numerical approximations of Hamilton Jacobi equations was first proposed for finite difference schemes in [10] and a generalized formulation was given in [4, 31]. Since then, various schemes were presented for Hamilton-Jacobi equations; high-order finite difference schemes in [6, 29, 26] and schemes for unstructured meshes [5, 30, 32, 2]. These methods are difficult to adapt to our problem. Indeed, the compatibility with the staggered schemes imposes a particular discretization of the gradient operator (discrete dual of the finite volume divergence) which is very different to the ones presented in the previous references. Besides, all the existing schemes proposed in the literature are designed to solve very generic Hamilton-Jacobi equations. In this paper, we only deal with a very particular operator, namely, $H(\boldsymbol{x})=\boldsymbol{u}\cdot\boldsymbol{x}+u_f|\boldsymbol{x}|$. Consequently, we propose a finite volume discretization of $u_f|\boldsymbol{\nabla}G|$ that is compatible with the staggered discretization of the transport operator $\boldsymbol{u}\cdot\boldsymbol{\nabla}G$.

For the sake of clarity, we focus on key elements of the discretization and we suppose that $\boldsymbol{u}=0$ and $u_f=1$, so the problem considered here is the unsteady eikonal equation,

$$\partial_t G+|\boldsymbol{\nabla}G|=0,\tag{1.6a}$$

$$G(0,\boldsymbol{x})=G_0(\boldsymbol{x}),\quad \forall\boldsymbol{x}\in\mathbb{R}^d,\tag{1.6b}$$

$G_0\in\mathrm{BUC}(\mathbb{R}^d)$. The choice of such a simplified model is also convenient as its analytical solutions can be computed easily (see Appendix (A) for more details). The scheme proposed to approximate this problem can be defined on unstructured meshes. On Cartesian grids, the scheme is consistent and monotone and the $L^\infty$ convergence is proved thanks to the theory developed in [4]. Numerical results are given to highlight this convergence results as well as the numerical convergence of the scheme on unstructured discretizations.

The discretization proposed in this paper has been implemented a Computational Fluid Dynamics software called P$^2$REMICS [22]. One of its purpose is to simulate the flame front propagation in the explosion phenomenon (the deflagration), for nuclear safety issues. The model involves partially premixed reactive flows. The G-equation (1.1) is used to determine the flame brush location. The unknown $G$ is a color function which separates the domain in burnt and unburnt subdomain. While $\boldsymbol{u}$ is an unknown of the problem representing the flow velocity, $u_f$ is a given scalar speed corresponding to the flame front propagation. It is a function that depend on multiple variables of the problem, among others, the combustion reaction, pressure and temperature. It is often tabulated from chemical solvers. The purpose is to condense the whole deflagration chemical process into one scalar data to lighten the global model. This equation is coupled with the system of balance laws (chemical species, momentum, energy, chemical mass fractions). The information from the $G$ function is added through the reactive source terms in the chemical mass fractions balance equation. More details about this model and the related results can be found in [14].

The paper is organized as follows. We start with the description of the spatial discretization and the corresponding notations that are used throughout the paper. We present the scheme and its properties in the second part. We finish with some convergence and numerical results.

## 2. Spatial discretization

In this section, we focus on the discretization of a multi-dimensional domain (*i.e.* $d = 2$ or $d = 3$); the simplification to the one-dimensional case is straightforward.

Let $\mathcal{M}$ be a mesh of the domain $\Omega$ (which is an open bounded connected subset of $\mathbb{R}^d$ or $\mathbb{R}^d$ itself), supposed to be regular in the usual sense of the finite element literature (*e.g.* [8]). The cells of the mesh are assumed to be:

- for a general domain $\Omega$, either non-degenerate quadrilaterals ($d = 2$) or hexahedra ($d = 3$) or simplices, both types of cells being possibly combined in a same mesh,
- for a domain whose boundaries are hyperplanes normal to a coordinate axis, rectangles ($d = 2$) or rectangular parallelepipeds ($d = 3$) (the faces of which, of course, are then also necessarily normal to a coordinate axis).

By $\mathcal{E}$ and $\mathcal{E}(K)$ we denote the set of all $(d-1)$-faces $\sigma$ of the mesh and of the element $K \in \mathcal{M}$ respectively. The set of faces included in the boundary of $\Omega$ is denoted by $\mathcal{E}_{\text{ext}}$ and the set of internal faces (*i.e.* $\mathcal{E} \setminus \mathcal{E}_{\text{ext}}$) is denoted by $\mathcal{E}_{\text{int}}$; a face $\sigma \in \mathcal{E}_{\text{int}}$ separating the cells $K$ and $L$ is denoted by $\sigma = K|L$. The outward normal vector to a face $\sigma$ of $K$ is denoted by $\boldsymbol{n}_{K,\sigma}$. For $K \in \mathcal{M}$ and $\sigma \in \mathcal{E}$, we denote by $|K|$ the measure of $K$ and by $|\sigma|$ the $(d-1)$-measure of the face $\sigma$. The mass center of a face is denoted by $\boldsymbol{x}_\sigma$, and $\boldsymbol{x}_K$ stands for the centroid of $K$.

Finally we denote by $d_\sigma$ the measure of $\overrightarrow{\boldsymbol{x}_K\boldsymbol{x}_L}$.

The unknown discrete function $G$ is piecewise constant on the cells $K$. We denote by $H_\mathcal{M}$ the space of such piecewise constant functions.

$$G_\mathcal{M} \in H_\mathcal{M} \Longleftrightarrow G_\mathcal{M} = \sum_{K \in \mathcal{M}} G_K \mathcal{X}_K,$$

where $\mathcal{X}_O$ stands for the characteristic function of the set $O$.

## 3. The scheme

The problem (1.6) is posed over $\mathbb{R}^d \times (0,T)$, where $(0,T)$ is a finite time interval. We suppose that we have $G_0 \in \mathrm{BUC}(\mathbb{R}^d)$. According to the known results at the continuous level, the problem has a unique viscosity solution in $\mathrm{BUC}([0,T] \times \mathbb{R}^d)$ that we denote $\bar{G}$. In order to be able to perform computations, the domain can be reduced to an open bounded connected subset $\Omega$ of $\mathbb{R}^d$ with zero-flux boundary conditions. Indeed, thanks to the finite speed of propagation property, one can ensure that the boundaries do not influence the solution within the computation time. We propose two versions of the scheme depending on the regularity of the mesh. The finite volume scheme is derived from an alternative form of Equation (1.6a) :

$$\partial_t G + \left(\frac{\boldsymbol{\nabla} G}{|\boldsymbol{\nabla} G|}\right) \cdot \boldsymbol{\nabla} G = 0. \tag{3.1}$$

We recall the classical Green's formula on each cell $K \in \mathcal{M}$, for $H^1(\Omega)$ functions $\boldsymbol{\psi}$ and $\phi$ :

$$\int_K \boldsymbol{\psi}.\boldsymbol{\nabla}\phi = \oint_{\partial K} (\phi\boldsymbol{\psi}) - \int_K \phi \mathrm{div}(\boldsymbol{\psi}). \tag{3.2}$$

This formula is used in the discrete case to derive a classical finite volume discretization of the divergence operator (see (3.6) below), from which we deduce a discretization of the term $\boldsymbol{\psi}.\boldsymbol{\nabla}\phi$. Usually, a $L^\infty(\Omega)$ and $\mathrm{BV}(\Omega)$ stability of the solution is observed on numerical computations, which leads to a $L^1$ norm control of the discrete gradient and divergence. Furthermore the Green formula is at least true in the weak sense in this case. We refer to [11, Chapter 1] for more details.

Let us consider a partition $0 = t_0 < t_1 < \ldots < t_N = T$ of the time interval $(0, T)$, which we suppose uniform for the sake of simplicity, and let $\delta t = t_{n+1} - t_n$ for $n = 0, 1, \ldots, N-1$ be the (constant) time step. We consider an explicit-in-time scheme, which reads, for $0 \leq n \leq N-1$ and $K \in \mathcal{M}$:

$$\eth_t G^n + F_{\mathcal{M}}(G^n) = 0, \tag{3.3}$$

with,

$$\eth_t G^n = \sum_{K\in\mathcal{M}} \frac{G_K^{n+1} - G_K^n}{\delta t} \mathcal{X}_K, \tag{3.4}$$

and

$$F_{\mathcal{M}}(G^n) = \sum_{K\in\mathcal{M}} \left\{ \mathrm{div}\left( \frac{\boldsymbol{\nabla}_{\mathcal{E}} G^n}{|\boldsymbol{\nabla}_{\mathcal{E}} G^n|} G^n \right)_K - G_K^n \mathrm{div}\left( \frac{\boldsymbol{\nabla}_{\mathcal{E}} G^n}{|\boldsymbol{\nabla}_{\mathcal{E}} G^n|} \right)_K \right\} \mathcal{X}_K. \tag{3.5}$$

The discrete divergence operator is given by:

$$\text{for } K \in \mathcal{M}, \qquad (\mathrm{div}\boldsymbol{u})_K = \frac{1}{|K|} \sum_{\sigma=K|L\in\mathcal{E}(K)} \kappa_{K,\sigma}^{\mathcal{M}} |\sigma|\ \boldsymbol{u}_\sigma.\boldsymbol{n}_{K,\sigma}, \tag{3.6}$$

where $\kappa_{K,\sigma}^{\mathcal{M}}$ is a coefficient equal to 1 for unstructured meshes and equal to $\kappa_{K,\sigma}^{\mathcal{M}} = \dfrac{2\ |K|}{|K| + |L|}$ on Cartesian grids. This coefficient is chosen so that, in the Cartesian case, $\dfrac{|\sigma|\kappa_{K,\sigma}^{\mathcal{M}}}{|K|} = \dfrac{1}{d_\sigma}$ which leads to a consistent discretization of the spatial operator as we will show hereafter. Likewise

$$\text{for } K \in \mathcal{M}, \qquad (\mathrm{div}\, G\boldsymbol{u})_K = \frac{1}{|K|} \sum_{\sigma=K|L\in\mathcal{E}(K)} \kappa_{K,\sigma}^{\mathcal{M}} |\sigma|\ G_\sigma \boldsymbol{u}_\sigma.\boldsymbol{n}_{K,\sigma}, \tag{3.7}$$

where $G_\sigma$ denotes an interpolation of $G$ on the edge $\sigma$ that is:

$$\text{for } \sigma = K|L \in \mathcal{E}_{\mathrm{int}}, \quad G_\sigma = \begin{vmatrix} G_K & \text{if } \boldsymbol{u}_\sigma.\boldsymbol{n}_{K,\sigma} \geq 0, \\ G_L & \text{otherwise.} \end{vmatrix}$$

The expression of the discrete spatial operator (3.5) becomes

$$F_{\mathcal{M}}(G_{\mathcal{M}}^n) = \sum_{K\in\mathcal{M}} \left[ \sum_{\sigma=K|L\in\mathcal{E}(K)} \kappa_{K,\sigma}^{\mathcal{M}} \frac{|\sigma|}{|K|} \frac{(\boldsymbol{\nabla}_{\mathcal{E}} G^n)_\sigma}{|(\boldsymbol{\nabla}_{\mathcal{E}} G^n)_\sigma|} \cdot \boldsymbol{n}_{K,\sigma} (G_\sigma^n - G_K^n) \right] \mathcal{X}_K, \tag{3.8}$$

where $\boldsymbol{\nabla}_{\mathcal{E}}$ refers to a discrete gradient operator defined on every $\sigma \in \mathcal{E}_{\mathrm{int}}$.

For a face $\sigma \in \mathcal{E}_{\mathrm{ext}}$ one simply takes $G_\sigma = G_K$ so that

$$\frac{|\sigma|}{|K|} (G_\sigma - G_K) = 0.$$

### 3.1. Unstructured meshes

For $\sigma = K|L \in \mathcal{E}_{\text{int}}$, we take:

$$(\boldsymbol{\nabla}_{\mathcal{E}} G)_\sigma = \sum_{\epsilon \in \partial(K \cup L)} \frac{|\epsilon|}{|K \cup L|} \tilde{G}_\epsilon \boldsymbol{n}_{K\cup L,\epsilon}, \tag{3.9}$$

with $\tilde{G}_\epsilon$ a second order approximation of $G$ at the centroid of the face $\epsilon$.

### 3.2. Cartesian meshes

When the scheme is based on Cartesian grids, an orthogonality condition is automatically satisfied, which leads to an easier way to obtain a consistent discretization of the component of the gradient collinear to the face. We have for $\sigma = \overrightarrow{K|L}$ (which means that $\boldsymbol{F} \cdot \boldsymbol{n}_{K,\sigma} \geq 0$ as in figure 3.1):

$$\text{For } \sigma \in \mathcal{E}_{\text{int}}, \qquad (\boldsymbol{\nabla}_{\mathcal{E}} G)_\sigma = \left[ \frac{G_L - G_K}{d_\sigma} \boldsymbol{n}_{K,\sigma} + \boldsymbol{\nabla}_{//\sigma} G \right], \tag{3.10}$$

where $\boldsymbol{\nabla}_{//\sigma}$ is defined by:

$$(\boldsymbol{\nabla} G)_{//\sigma} = \sum_{\substack{i=1, \\ \boldsymbol{e}^{(i)} \cdot \boldsymbol{n}_{K,\sigma} = 0}}^{d} \left\{ \frac{(G_{K_i^+} - G_K)^+}{d_{\sigma_i^+}} - \frac{1}{2} \left( 1 - \operatorname{sgn}(G_{K_i^+} - G_K)^+ \right) \frac{(G_K - G_{K_i^-})^-}{d_{\sigma_i^-}} \right\} \boldsymbol{e}^{(i)}, \tag{3.11}$$

with $\sigma = \overrightarrow{K|L}$. For a cell $K \in \mathcal{M}$, $\sigma_i^+$ and $\sigma_i^-$ stand for the two faces of $K$ normal to $\boldsymbol{e}^{(i)}$. Superscripts $-$ and $+$ refer to the up and down faces of $K$ respectively. We set $\sigma_i^+ = K|K_i^+$ and $\sigma_i^- = K|K_i^-$. We illustrate these notations in figure 3.1. We recall that $a^+ = \max(a, 0)$ and $a^- = \max(-a, 0)$, for $a \in \mathbb{R}$. This particular discretization is important to derive some monotonicity property.

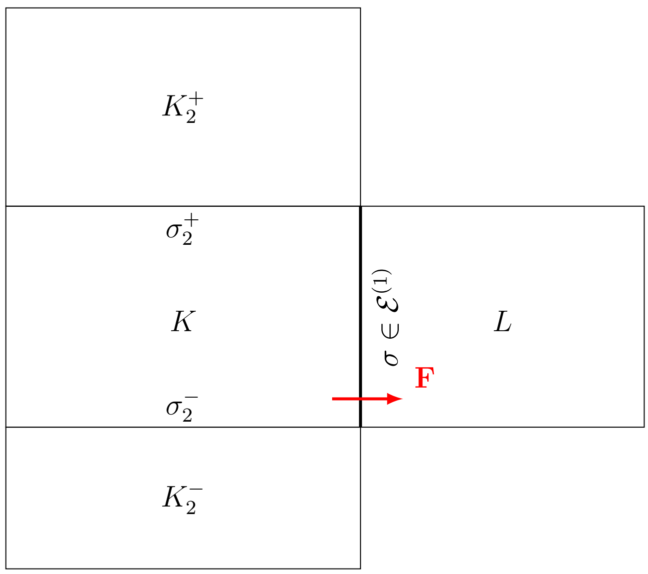


Figure 3.1. Notations for the alternative gradient definition on Cartesian grids with $\mathbf{F} = (G_L - G_K)\boldsymbol{n}_{K,\sigma}$.

### 3.3. High order extension

It is possible to replace the upwind interpolation by a higher order interpolation based on a MUSCL reconstruction. Adopting the same notations as in (3.7), its important property, based on [28] is stated below. For any $K \in \mathcal{M}$, and for any $\sigma \in \mathcal{E}(K) \cap \mathcal{E}_{\text{int}}$, there exists $\beta_{K,\sigma} \in [0,1]$, and a neighbouring cell of $K$ denoted $M_\sigma^K$, such that:

$$G_\sigma - G_K = \left| \begin{array}{ll} \beta_{K,\sigma}(G_K - G_{M_\sigma^K}) & \text{if } \dfrac{\boldsymbol{\nabla}_{\mathcal{E}} G_\sigma}{|\boldsymbol{\nabla}_{\mathcal{E}} G_\sigma|} \cdot \boldsymbol{n}_{K,\sigma} \geq 0, \\ \beta_{K,\sigma}(G_{M_\sigma^K} - G_K) & \text{otherwise.} \end{array} \right. \tag{3.12}$$

The procedure to obtain such interpolation is the following:

- Define a tentative value $\tilde{G}_\sigma$ based on a high order geometric interpolation.
- Create a limitation procedure for $G_\sigma$. Let $\sigma \in \mathcal{E}_{\text{int}}$, $\sigma = \overrightarrow{K|L}$ and $V_K$ be a set of neighboring cells to $K$. Define the two following limitation intervals:

$$\begin{aligned} &(H1) \quad G_\sigma - G_K \in |[0, \tfrac{\zeta^+}{2}\,(G_L - G_K)]|, \\ &(H2) \quad \exists M \in V_K,\, G_\sigma - G_K \in |[0, \tfrac{\zeta^-}{2}\,\tfrac{d_\sigma}{d_{K|M}}\,(G_K - G_M)]|, \end{aligned} \tag{3.13}$$

  where, $d_{K|M}$ stands for the measure of $|\overrightarrow{\boldsymbol{x}_K \boldsymbol{x}_M}|$. For $a, b \in \mathbb{R}$, we denote by $|[a,b]|$ the ordered interval of $a$ and $b$ and $\overrightarrow{K|L}$ means that the gradient of $G$ and the normal to the face outward of $K$ make an acute angle $(\dfrac{\boldsymbol{\nabla}_{\mathcal{E}} G_\sigma}{|\boldsymbol{\nabla}_{\mathcal{E}} G_\sigma|}.\boldsymbol{n}_{K,\sigma} \geq 0)$. The parameters $\zeta^+$ and $\zeta^-$ lie in $[0,2]$.

- Compute $G_\sigma$ as the nearest point to $\tilde{G}_\sigma$ in the limitation interval.

Whenever it is possible (*i.e.* with a mesh obtained by $Q_1$ mappings from the $(0,1)^d$ reference element), $V_K$ may be chosen as the opposite cells to $\sigma$ in $K$. Otherwise $V_K$ is defined as the set of "upstream cells" to $K$. Note that, for a structured mesh, the first choice allows to recover the usual minmod limiter. We refer to [13] for more details on the procedure.

**Remark 3.1** (Cartesian grids)**.** We impose $\zeta^+ = \zeta^- = 1$ for the Cartesian version of the scheme. This particular choice of parameters is the only one possible if we want to get consistency properties for the discrete spatial operator of the scheme.

## 4. Properties of the scheme

We expose in this section the properties of the scheme. A specific paragraph is devoted to its additional properties on Cartesian grids, derived from the convergence theory [4, 31]. This ensures that the given discretization behaves like usual finite difference methods for Hamilton-Jacobi equations.

### 4.1. Stability

Thanks to the definition of the discrete convective operator, we have the following property:

**Proposition 4.1** (Maximum principle on non-Cartesian grids)**.** *Let $G^n_{\mathcal{M}} \in H_{\mathcal{M}}$, $n \in [0, N]$, be the solution of the scheme* (3.3)*. For all $K \in \mathcal{M}$ and $n \in [0, N-1]$, we have:*

$$\min_{L \in \mathcal{M}} G^n_L \leq G^{n+1}_K \leq \max_{L \in \mathcal{M}} G^n_L,$$

*under the CFL condition:*

$$\delta t \leq \min_{K \in \mathcal{M}} \frac{|K|}{\sum\limits_{\sigma \in \mathcal{E}(K)} |\sigma|}. \tag{4.1}$$

**Proof.** We have, for $K \in \mathcal{M}$ and $n \in [0, N-1]$:

$$G_K^{n+1} = \left(1 - \delta t \sum_{\sigma \in \mathcal{E}(K)} \frac{|\sigma|}{|K|} \left( \frac{\boldsymbol{\nabla}_{\mathcal{E}} G_\sigma^n}{|\boldsymbol{\nabla}_{\mathcal{E}} G_\sigma^n|} \cdot \boldsymbol{n}_{K,\sigma} \right)^- \right) G_K^n + \delta t \sum_{\sigma = K|L \in \mathcal{E}(K)} \frac{|\sigma|}{|K|} \left( \frac{\boldsymbol{\nabla}_{\mathcal{E}} G_\sigma^n}{|\boldsymbol{\nabla}_{\mathcal{E}} G_\sigma^n|} \cdot \boldsymbol{n}_{K,\sigma} \right)^- G_L^n.$$

Consequently, $G_K^{n+1}$ is a convex combination of its neighbors at time $n$ if (4.1) is verified, which completes the proof. ∎

**Remark 4.2** (Cartesian grids)**.** The property remains the same with the scheme on Cartesian grids, only the CFL is modified. One must replace $|K|$ by $\frac{|K|+|L|}{2}$ in (4.1).

**Remark 4.3** (MUSCL interpolation)**.** Concerning the MUSCL interpolation, we use the property (3.12) in the scheme to get:

$$G_K^{n+1} = \left(1 - \delta t \sum_{\sigma \in \mathcal{E}(K)} \frac{|\sigma|}{|K|} \beta_{K,\sigma} \left| \frac{\boldsymbol{\nabla}_{\mathcal{E}} G_\sigma^n}{|\boldsymbol{\nabla}_{\mathcal{E}} G_\sigma^n|} \cdot \boldsymbol{n}_{K,\sigma} \right| \right) G_K^n + \delta t \sum_{\sigma \in \mathcal{E}(K)} \frac{|\sigma|}{|K|} \beta_{K,\sigma} \left| \frac{\boldsymbol{\nabla}_{\mathcal{E}} G_\sigma^n}{|\boldsymbol{\nabla}_{\mathcal{E}} G_\sigma^n|} \cdot \boldsymbol{n}_{K,\sigma} \right| G_{M_K^\sigma}^n.$$

The maximum principle is still satisfied with the same CFL condition.

### 4.2. Invariance under translation

**Proposition 4.4** (Invariance under Translation with constants)**.**
$\forall \lambda \in \mathbb{R}$ *and* $\forall \phi_{\mathcal{M}} \in H_{\mathcal{M}}$,

$$F_{\mathcal{M}}(\phi_{\mathcal{M}} + \lambda) = F_{\mathcal{M}}(\phi_{\mathcal{M}}). \tag{4.2}$$

**Proof.** Let $\lambda \in \mathbb{R}$ and $\phi_{\mathcal{M}} \in H_{\mathcal{M}}$. Looking at (3.8), we need to check that $\boldsymbol{\nabla}_{\mathcal{E}} (\phi_{\mathcal{M}} + \lambda) = \boldsymbol{\nabla}_{\mathcal{E}} \phi_{\mathcal{M}}$. We remind that:

$$\boldsymbol{\nabla}_{\mathcal{E}} (\phi_{\mathcal{M}} + \lambda) = \sum_{\sigma \in \partial(K \cup L)} \frac{|\sigma|}{|K \cup L|} (\phi_\sigma + \lambda) \, \boldsymbol{n}_{K \cup L, \sigma}.$$

We have:

$$\boldsymbol{\nabla}_{\mathcal{E}} (\phi_{\mathcal{M}} + \lambda) = \boldsymbol{\nabla}_{\mathcal{E}} \phi_{\mathcal{M}} + \lambda \sum_{\sigma \in \partial(K \cup L)} \frac{|\sigma|}{|K \cup L|} \boldsymbol{n}_{K \cup L, \sigma}.$$

Using the divergence theorem, we get that:

$$\sum_{\sigma \in \partial K \cup L} \frac{|\sigma|}{|K \cup L|} \boldsymbol{n}_{K \cup L, \sigma} = \int_{K \cup L} \boldsymbol{\nabla}(1) = 0,$$

which concludes the proof. ∎

On Cartesian meshes, the result is immediate.

### 4.3. Properties of the Cartesian scheme

We now state within this paragraph two important results verified by the scheme on Cartesian grids only. These are obtained thanks to the orthogonality properties verified by Cartesian grids.

4.3.1. *Consistency*

We need to define interpolates of test functions on the mesh. Let $\phi \in C_c^\infty(\Omega)$. We set:

$$\phi_{\mathcal{M}} = \sum_{K \in \mathcal{M}} \phi_K \mathcal{X}_K \ \in H_{\mathcal{M}}, \qquad \phi_K = \phi(\boldsymbol{x}_K). \tag{4.3}$$

We now give the definition of the consistency property.

**Definition 4.5** (Consistency)**.** Let $F$ be an operator approximated by $F_{\mathcal{M}}$. Let $h_{\mathcal{M}} = \max_{K \in \mathcal{M}} \operatorname{diam}(K)$. Let $\mathcal{D}^{(m)} = \left\{\mathcal{M}^{(m)}, \mathcal{E}^{(m)}\right\}$ be a sequence of discretizations such that the size $h_{\mathcal{M}}^{(m)}$ tends to zero as $m \to \infty$. The discrete spatial operator $F_{\mathcal{M}}$ is said to be consistent with $F$ if, for every $\phi \in C_c^\infty(\Omega)$:

$$\lim_{m \to \infty} \|F_{\mathcal{M}^{(m)}}(\phi_{\mathcal{M}^{(m)}}) - F(\phi)\|_{L^\infty(\Omega)} = 0.$$

The next proposition states the consistency of the spatial discretization in the Cartesian case.

**Proposition 4.6.** *The spatial operator in the Cartesian case, given by, for $G_{\mathcal{M}} \in H_{\mathcal{M}}$:*

$$F_{\mathcal{M}}(G_{\mathcal{M}}) = \sum_{K \in \mathcal{M}} \left[ \sum_{\sigma = K|L \in \mathcal{E}(K)} \frac{1}{d_\sigma} \frac{(G_L - G_K)}{\sqrt{(G_L - G_K)^2 + d_\sigma^2 |\boldsymbol{\nabla}_{//\sigma} G_{\mathcal{M}}|^2}} (G_\sigma - G_K) \right] \mathcal{X}_K, \tag{4.4}$$

*with $\boldsymbol{\nabla}_{//\sigma}$ defined in* (3.11)*, is consistent with $|\boldsymbol{\nabla} G|$.*

**Proof.** Let $\phi \in C_c^\infty(\Omega)$ and $\phi_{\mathcal{M}} \in H_{\mathcal{M}}$ its interpolation on the mesh. Consider $K \in \mathcal{M}$ and $\boldsymbol{v}$ a constant vector. Let $\tilde{F}_K(\phi_{\mathcal{M}}, \boldsymbol{v})$ be defined by:

$$\tilde{F}_K(\phi_{\mathcal{M}}, \boldsymbol{v}) = \sum_{\sigma = K|L \in \mathcal{E}(K)} \frac{1}{d_\sigma} (\boldsymbol{v} \cdot \boldsymbol{n}_{K,\sigma})(\phi_\sigma - \phi_K).$$

With the upwind interpolation, we get that:

$$\tilde{F}_K(\phi_{\mathcal{M}}, \boldsymbol{v}) = -\sum_{\sigma = K|L \in \mathcal{E}(K)} \frac{1}{d_\sigma} (\boldsymbol{v} \cdot \boldsymbol{n}_{K,\sigma})^- (\phi_L - \phi_K).$$

A simple Taylor expansion leads to:

$$\tilde{F}_K(\phi_{\mathcal{M}}, \boldsymbol{v}) = -\sum_{\sigma = K|L \in \mathcal{E}(K)} (\boldsymbol{v} \cdot \boldsymbol{n}_{K,\sigma})^- \boldsymbol{\nabla}\phi(\boldsymbol{x}_K).\boldsymbol{n}_{K,\sigma} + \mathcal{O}(h_{\mathcal{M}}),$$

so

$$\tilde{F}_K(\phi_{\mathcal{M}}, \boldsymbol{v}) = \boldsymbol{\nabla}\phi(\boldsymbol{x}_K) \cdot \sum_{\sigma = K|L \in \mathcal{E}(K)} (\boldsymbol{v} \cdot \boldsymbol{n}_{L,\sigma})^+ \boldsymbol{n}_{L,\sigma} + \mathcal{O}(h_{\mathcal{M}}).$$

Thanks to the orthogonality condition verified by Cartesian grids, we have:

$$\sum_{\sigma = K|L \in \mathcal{E}(K)} (\boldsymbol{v} \cdot \boldsymbol{n}_{L,\sigma})^+ \boldsymbol{n}_{L,\sigma} = \sum_{i=1}^{d} (\boldsymbol{v} \cdot \boldsymbol{e}^{(i)}) \boldsymbol{e}^{(i)} = \boldsymbol{v},$$

so we have:

$$\tilde{F}_K(\phi_{\mathcal{M}}, \boldsymbol{v}) = \boldsymbol{v} \cdot \boldsymbol{\nabla}\phi(\boldsymbol{x}_K) + \mathcal{O}(h_{\mathcal{M}}).$$

Concerning the MUSCL interpolation, we have:

$$\begin{aligned}\tilde{F}_K(\phi_{\mathcal{M}}, \boldsymbol{v}) = \frac{1}{2} \sum_{\sigma=K|L\in\mathcal{E}(K)} & \frac{1}{d_\sigma}(\boldsymbol{v}\cdot\boldsymbol{n}_{K,\sigma})^+ \min\left(\phi_K - \phi_{M_K^\sigma}\frac{d_\sigma}{d_{K|M_K^\sigma}}, \phi_L - \phi_K\right) \\ & - \sum_{\sigma=K|L\in\mathcal{E}(K)} (\boldsymbol{v}\cdot\boldsymbol{n}_{K,\sigma})^-(\phi_L - \phi_K) \\ & - \frac{1}{2}\sum_{\sigma=K|L\in\mathcal{E}(K)} \frac{1}{d_\sigma}(\boldsymbol{v}\cdot\boldsymbol{n}_{K,\sigma})^- \min\left(\phi_L - \phi_{M_L^\sigma}\frac{d_\sigma}{d_{L|M_L^\sigma}}, \phi_K - \phi_L\right),\end{aligned}$$

where $M_K^\sigma$ refers to the opposite cell to $\sigma$ in $K$. It is easy to see that:

$$\frac{1}{d_\sigma}\min\left(\phi_K - \phi_{M_K^\sigma}\frac{d_\sigma}{d_{K|M_K^\sigma}}, \phi_L - \phi_K\right) = \boldsymbol{\nabla}\phi(\boldsymbol{x}_K)\cdot\boldsymbol{n}_{K,\sigma} + \mathcal{O}(h_{\mathcal{M}}),$$

and,

$$\frac{1}{d_\sigma}\min\left(\phi_L - \phi_{M_L^\sigma}\frac{d_\sigma}{d_{L|M_L^\sigma}}, \phi_K - \phi_L\right) = \boldsymbol{\nabla}\phi(\boldsymbol{x}_K)\cdot\boldsymbol{n}_{L,\sigma} + \mathcal{O}(h_{\mathcal{M}}).$$

Therefore,

$$\tilde{F}_K(\phi_{\mathcal{M}}, \boldsymbol{v}) = \frac{1}{2}\sum_{\sigma\in\mathcal{E}(K)} (\boldsymbol{v}\cdot\boldsymbol{n}_{K,\sigma})^+\boldsymbol{\nabla}\phi(\boldsymbol{x}_K)\cdot\boldsymbol{n}_{K,\sigma} + \frac{1}{2}\sum_{\sigma\in\mathcal{E}(K)} (\boldsymbol{v}\cdot\boldsymbol{n}_{L,\sigma})^+\boldsymbol{\nabla}\phi(\boldsymbol{x}_K)\cdot\boldsymbol{n}_{L,\sigma} + \mathcal{O}(h_{\mathcal{M}}),$$

which leads to:

$$\begin{aligned}\tilde{F}_K(\phi_{\mathcal{M}}, \boldsymbol{v}) &= \boldsymbol{\nabla}\phi(\boldsymbol{x}_K)\cdot \sum_{\sigma=K|L\in\mathcal{E}(K)} \frac{1}{2}\left((\boldsymbol{v}\cdot\boldsymbol{n}_{K,\sigma})^+\boldsymbol{n}_{K,\sigma} + (\boldsymbol{v}\cdot\boldsymbol{n}_{L,\sigma})^+\boldsymbol{n}_{L,\sigma}\right) + \mathcal{O}(h_{\mathcal{M}}) \\ &= \boldsymbol{\nabla}\phi(\boldsymbol{x}_K)\cdot\boldsymbol{v} + \mathcal{O}(h_{\mathcal{M}}).\end{aligned}$$

Noticing, thanks to the consistency of $\boldsymbol{\nabla}_{\mathcal{E}}$, that:

$$F_{\mathcal{M}}(\phi_{\mathcal{M}}) = \sum_{K\in\mathcal{M}} \tilde{F}_K\left(\phi_{\mathcal{M}}, \frac{\boldsymbol{\nabla}\phi(\boldsymbol{x}_K)}{|\boldsymbol{\nabla}\phi(\boldsymbol{x}_K)|}\right)\mathcal{X}_K + \mathcal{O}(h_{\mathcal{M}}),$$

we can deduce that:

$$\lim_{m\to\infty} \|F_{\mathcal{M}}(\phi_{\mathcal{M}}) - |\boldsymbol{\nabla}\phi|\|_{L^\infty(\Omega)} = 0,$$

which concludes the proof. ∎

4.3.2. *Monotonicity*

Let $(\phi_{\mathcal{M}}, \psi_{\mathcal{M}}) \in H^2_{\mathcal{M}}$. Let us define the following partial order

$$\phi_{\mathcal{M}} \le \psi_{\mathcal{M}} \qquad \Longleftrightarrow \qquad \forall K\in\mathcal{M}, \quad \phi_K \le \psi_K. \tag{4.5}$$

Then we get the following result with the Cartesian upwind scheme only.

**Proposition 4.7** (Monotonicity of the upwind Cartesian scheme)**.**
*Suppose that the following CFL condition is satisfied*

$$\delta t \le \frac{1}{\sum_{\sigma\in\mathcal{E}(K)} \frac{1+\frac{1}{2}\sqrt{1+r_K^2}}{d_\sigma}}, \qquad r_K = \max_{(\sigma,\sigma')\in\mathcal{E}(K)} \frac{d_\sigma}{d_{\sigma'}}. \tag{4.6}$$

*Then we have the following result:*

$$\forall(\phi_{\mathcal{M}}, \psi_{\mathcal{M}}) \in H^2_{\mathcal{M}}, \qquad \phi_{\mathcal{M}} \le \psi_{\mathcal{M}} \implies \phi_{\mathcal{M}} + \delta t\ F_{\mathcal{M}}(\phi_{\mathcal{M}}) \le \psi_{\mathcal{M}} + \delta t\ F_{\mathcal{M}}(\psi_{\mathcal{M}}).$$

**Proof.** For the sake of clarity we prove the result in dimension $d = 2$. The extension to dimension $d = 3$ can be performed in a similar manner but at the cost of more complicated computations and heavier expressions. We can equivalently check that $SCH(\phi_{\mathcal{M}}) := \phi_{\mathcal{M}} + F_{\mathcal{M}}(\phi_{\mathcal{M}})$ is a non decreasing function of each variable. Let $K \in \mathcal{M}$ and $\phi_{\mathcal{M}} \in H_{\mathcal{M}}$. We have:

$$SCH(\phi_{\mathcal{M}})|_K = \phi_K + \delta t \sum_{\sigma=K|L\in\mathcal{E}(K)} \frac{1}{d_\sigma} f_{K,\sigma}\left(\phi_{\mathcal{M}}\right),$$

with,

$$f_{K,\sigma}\left(\phi_{\mathcal{M}}\right) = \frac{(\phi_L - \phi_K)^-}{\sqrt{(\phi_L - \phi_K)^2 + d_\sigma^2 |\boldsymbol{\nabla}_{//\sigma}\phi_{\mathcal{M}}|^2}}(\phi_L - \phi_K).$$

The monotonicity of $f_{K,\sigma}$ with respect to $\phi_L$ is equivalent to the monotonicity of the function:

$$f : x \longmapsto \frac{x^- x}{|x|} = -x^-, \quad \forall x \in \mathbb{R},$$

because $\boldsymbol{\nabla}_{//\sigma}\phi_{\mathcal{M}}$ does not depend on $\phi_L$ in the Cartesian case (see (3.11)). We can conclude that $f_{K,\sigma}$ is a non decreasing function of $\phi_L$. Concerning the monotonicity in $\phi_{K^-}$ and $\phi_{K^+}$ it is equivalent to the variations of:

$$f : x \longmapsto -\frac{1}{x^+},$$

which is a non decreasing function. We can conclude that $SCH(\phi_{\mathcal{M}})|_K$ is an increasing function of each $(\phi_M)_{\substack{M\in\mathcal{M}\\ M\neq K}}$. Concerning $\phi_K$, we have:

$$SCH(\phi_{\mathcal{M}})|_K = g(\phi_K) = \phi_K - \delta t \sum_{\sigma=K|L\in\mathcal{E}(K)} \frac{1}{d_\sigma} \frac{(\phi_K - \phi_L)^+(\phi_K - \phi_L)}{\sqrt{(\phi_L - \phi_K)^2 + d_\sigma^2 |\boldsymbol{\nabla}_{//\sigma}\phi_{\mathcal{M}}|^2}}.$$

The analysis of this function can be split into three cases. If, $\forall \sigma \in \mathcal{E}(K)$, $\phi_K \le \phi_L$, then $g(\phi) = \phi_K$ which is non decreasing. The second case is when, $\forall \sigma \in \mathcal{E}(K)$, $\phi_K \ge \max(\phi_{K^+},\ \phi_{K^-},\ \phi_L)$. We have:

$$g(\phi_K) = \phi_K - \sum_{\sigma=K|L\in\mathcal{E}(K)} \frac{\delta t}{d_\sigma}\left(\phi_K - \phi_L\right),$$

which is non decreasing if,

$$\delta t \le \frac{1}{\sum_{\sigma\in\mathcal{E}(K)} d_\sigma^{-1}}.$$

We notice that this condition is satisfied if the CFL condition (4.6) is fulfilled. Finally, suppose that $\forall \sigma \in \mathcal{E}(K)$, $\phi_L \le \phi_K \le \phi_{K^+}$ (or $\phi_{K^-}$), we have, denoting by $r_\sigma = \frac{d_\sigma}{d_{\sigma^+}}$ :

$$g(\phi_K) = \phi_K - \delta t \sum_{\sigma=K|L\in\mathcal{E}(K)} \frac{1}{d_\sigma} \frac{\phi_K - \phi_L}{\sqrt{(\phi_K - \phi_L)^2 + r_\sigma^2(\phi_K - \phi_{K^+})^2}}(\phi_K - \phi_L).$$

Let us differentiate this function with respect to $\phi_K$:

$$\begin{aligned} g'(\phi_K) = 1 - \delta t &\sum_{\sigma=K|L\in\mathcal{E}(K)} \frac{1}{d_\sigma} \frac{\phi_K - \phi_L}{\sqrt{(\phi_K - \phi_L)^2 + r_\sigma^2(\phi_K - \phi_{K^+})^2}} \\ &- \delta t \sum_{\sigma=K|L\in\mathcal{E}(K)} \frac{1}{d_\sigma} \frac{r_\sigma^2(\phi_K - \phi_{K^+})(\phi_K - \phi_L)(\phi_L - \phi_{K^+})}{\left((\phi_K - \phi_L)^2 + r_\sigma^2(\phi_K - \phi_{K^+})^2\right)^{3/2}}. \end{aligned}$$

One can notice directly that:

$$\frac{\phi_K - \phi_L}{\sqrt{(\phi_K - \phi_L)^2 + r_\sigma^2(\phi_K - \phi_{K^+})^2}} \le 1.$$

In order to bound by above the second sum, we analyze the function

$$h : x \longmapsto \frac{r^2 x(a-x)a}{(x^2+r^2(a-x)^2)^{3/2}},$$

where $a, r$ are strictly positive constants. We split the function in two parts $h(x) = h_1(x)h_2(x)$ with:

$$\begin{aligned} h_1(x) =& \frac{r^2 x(a-x)}{x^2+r^2(a-x)^2}, \\ h_2(x) =& \frac{a}{\sqrt{x^2+r^2(a-x)^2}}. \end{aligned}$$

Concerning $h_1$ we can equivalently consider the function defined on $\mathbb{R}^+$ by:

$$y \longmapsto \frac{r^2}{y+\frac{r^2}{y}} = \frac{r^2 y}{y^2+r^2}.$$

A quick study of the function shows that,

$$\max_{y\in\mathbb{R}^+} \frac{r^2 y}{y^2+r^2} = \frac{r}{2} = \max_{x\in[0,a]} h_1(x).$$

The same work is performed with $h_2$ and leads to:

$$\max_{x\in[0,a]} h_2(x) = \frac{\sqrt{1+r^2}}{r}.$$

Gathering the results, we get that:

$$\forall x \in [0,a], \quad h(x) \leq \frac{1}{2}\sqrt{1+r^2}.$$

As a result, writing out $r = r_K = \max\limits_{(\sigma,\sigma')\in\mathcal{E}(K)} \dfrac{d_\sigma}{d_{\sigma'}}$, we have

$$g'(\phi_K) \geq 1 - \delta t \sum_{\sigma\in\mathcal{E}(K)} \frac{1+\frac{1}{2}\sqrt{1+r_K^2}}{d_\sigma},$$

so $g'(\phi_K) \geq 0$ provided that (4.6) is satisfied. This CFL condition ensures that $\phi_{\mathcal{M}} + \delta t\ F_{\mathcal{M}}(\phi_{\mathcal{M}})|_K$ is a non decreasing function of $\phi_K$, which concludes the proof. ■

**Remark 4.8.** All the results proved here can be extended with a transport velocity $\boldsymbol{u} \neq 0$ and a front propagation speed $u_f \neq 1$. Only the CFL conditions are modified, the sketches of the proofs are the same. One can suppose a general CFL condition of the form:

$$1 - \delta t \sum_{\sigma\in\mathcal{E}(K)} \frac{|\sigma|}{|K|}|\boldsymbol{u}_\sigma^n| + |(uf)_\sigma| \frac{1+\frac{1}{2}\sqrt{1+r_K^2}}{d_\sigma} \geq 0,$$

for all $K \in \mathcal{M}$, $\sigma \in \mathcal{E}(K)$ and $n = 0..N$. However the monotonicity results have not been extended to the MUSCL interpolation, and more generally to the non Cartesian case.

**Remark 4.9.** One can see that the CFL condition gets more restrictive as $r_K$ increases. Indeed $r_K$ is an indicator of the regularity of the mesh ; high values imply flattened cells. For uniform Cartesian grids $d_\sigma = h$ and $r_K = 1$ for all $K \in \mathcal{M}$ and $\sigma \in \mathcal{E}$, and the CFL condition boils down to $\dfrac{\delta t}{h} \leq \dfrac{1}{4+2\sqrt{2}} \approx \dfrac{1}{6.8}$.

## 5. A convergence result in the Cartesian case

The previous section ensures that the upwind scheme satisfies the basic properties to seek a convergence result on Cartesian meshes. We first recall the theorem given in [4], adapted to our notations.

**Theorem 5.1.** *Let $\bar{G}$ be the viscosity solution of* (1.6). *Let $\mathcal{D}^{(m)} = \left\{\mathcal{M}^{(m)}, \mathcal{E}^{(m)}, \delta t^{(m)}\right\}$ be a sequence of discretizations such that the space and time steps tend to zero as $m \to \infty$. Consider the following explicit scheme, for $n \in [0, N-1]$:*

$$\eth_t G_m^n + F_{\mathcal{M}}(G_m^n) = 0,$$

*with $\eth_t$ and $F_{\mathcal{M}}$ defined in* (3.4) *and* (3.8) *respectively, and the complete solution defined by $G_m^{(T)} = \sum_{n=0}^{N-1} G_m^{n+1} \mathcal{X}_{[t^n, t^{n+1}]}$. We suppose that:*

- *The spatial operator $F_{\mathcal{M}}$ is consistent with the continuous operator $G \longmapsto |\boldsymbol{\nabla} G|$.*
- *The scheme is invariant under translations: $F_{\mathcal{M}}(G_{\mathcal{M}} + v) = F_{\mathcal{M}}(G_{\mathcal{M}})$, $\forall v \in \mathbb{R}$.*
- *The scheme is monotone.*

*Then,*

$$G_m^{(T)} \longrightarrow \bar{G} \text{ uniformly as } m \to \infty.$$

The key ideas to prove this theorem can be found in [10]. Since we have shown the required assumptions of theorem 5.1, we can thus conclude to the convergence of the scheme, which we state in the following corollary.

**Corollary 5.2.** *Let $\bar{G}$ be the viscosity solution of* (1.6). *Let $\mathcal{D}^{(m)} = \left\{\mathcal{M}^{(m)}, \mathcal{E}^{(m)}, \delta t^{(m)}\right\}$ be a sequence of Cartesian discretizations such that the space and time steps tend to zero as $m \to \infty$. Now suppose there exists $r > 0$, such that $\forall m \in \mathbb{N}$, $\forall (\sigma, \sigma') \in \mathcal{E}^{(m)}$,*

$$\frac{d_\sigma}{d_{\sigma'}} \leq r.$$

*Suppose that, for any $m \in \mathbb{N}$,*

$$\delta t^{(m)} \leq \max_{K \in \mathcal{M}^{(m)}} \frac{1}{\sum_{\sigma \in \mathcal{E}(K)} \frac{1 + \frac{1}{2}\sqrt{1 + r^2}}{d_\sigma}}.$$

*Then the solution of the upwind Cartesian scheme* (3.3)-(4.4) *$G_m^{(T)}$ converges uniformly towards $\bar{G}$.*

**Remark 5.3.** The scheme could be extended to a wider class of Hamilton-Jacobi equations. Indeed one can see that any Hamiltonian of the form $H(\boldsymbol{\nabla} G) = \mathbf{F}(\boldsymbol{\nabla} G) \cdot \boldsymbol{\nabla} G$ could be discretized as follows :

$$F_{\mathcal{M}}(G_{\mathcal{M}}) = \sum_{K \in \mathcal{M}} \left[ \sum_{\sigma = K|L \in \mathcal{E}(K)} \kappa_{K,\sigma}^{\mathcal{M}} \frac{|\sigma|}{|K|} \, \mathbf{F}((\boldsymbol{\nabla}_{\mathcal{E}} G)_\sigma) \cdot \boldsymbol{n}_{K,\sigma} (G_\sigma - G_K) \right] \mathcal{X}_K,$$

The scheme would still guarantee some properties such as the maximum principle. On Cartesian grids, the consistency can be easily obtained but the monotonicity will be strongly dependent on the shape of $\mathbf{F}$.

In particular, the numerical analysis presented in the previous section can be applied to the case of a quadratic Hamiltonian $H(\nabla G) = \dfrac{1}{2}|\nabla G|^2$. Besides in the case of more regular meshes, namely when $\overrightarrow{\boldsymbol{x}_K\boldsymbol{x}_L}$ is collinear to $\boldsymbol{n}_{K,\sigma}$ (often called admissible meshes), taking

$$(\nabla'_{\mathcal{E}}G)_\sigma = \frac{G_L - G_K}{d_\sigma}\boldsymbol{n}_{K,\sigma} + (\nabla_{\mathcal{E}}G)^{\perp}_{\sigma},$$

with $(\nabla_{\mathcal{E}}G)^{\perp}_{\sigma}$ the projection of the gradient (3.9) on $\mathrm{Span}(\boldsymbol{n}_{K,\sigma})^{\perp}$, will also ensure the monotonicity property.

## 6. Numerical results

In this section we present numerical tests to highlight the properties of the numerical scheme and to compare it with a classical upwind finite difference scheme. The first paragraph is devoted to 1D computations.

### 6.1. One dimension

The domain is $\Omega = (0, 1)$. We use zero-flux boundary conditions at $x = 0$ and $x = 1$. We suppose that the time and space steps are constant for simplicity. Consider the following initial data:

$$G_0(x) = |\sin(4\pi x)|. \tag{6.1}$$

We plot the solution at $T = 0.05s$, with an upwind interpolation for the spatial operator, and a fixed CFL number equal to $\frac{\delta t}{h} = 1/10$ on figure 6.1 (One notice that (4.1) is satisfied thanks to the remark 4.9).

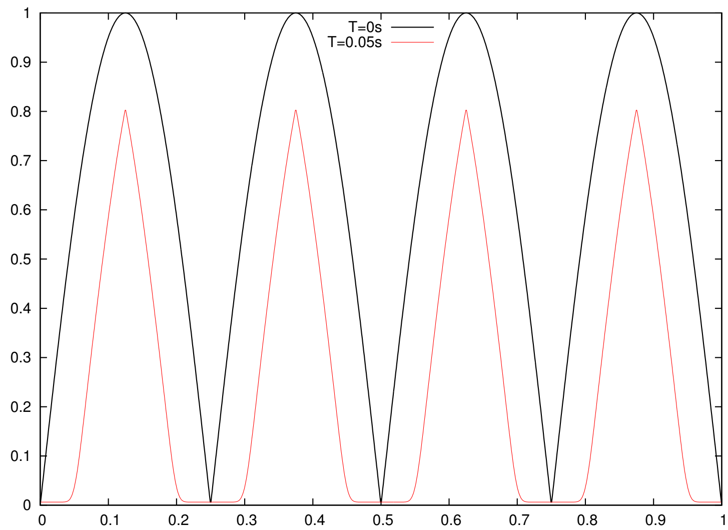


Figure 6.1. Solution of the G-equation with the upwind scheme at $T = 0.05s$.

It is possible to determine the unique viscosity solution of the eikonal equation for a given bounded uniformly continuous initial data. The expression of the solution is given by (A.1) and its proof can be found in the Appendix (A). Consequently we can highlight numerically the theoretical result about the convergence of the solution of our scheme towards the viscosity solution. Figure 6.2 below gives the error in $L^1$ norm with respect to the space step, in a log-log scale, for a fixed CFL number equal to $\frac{1}{10}$.

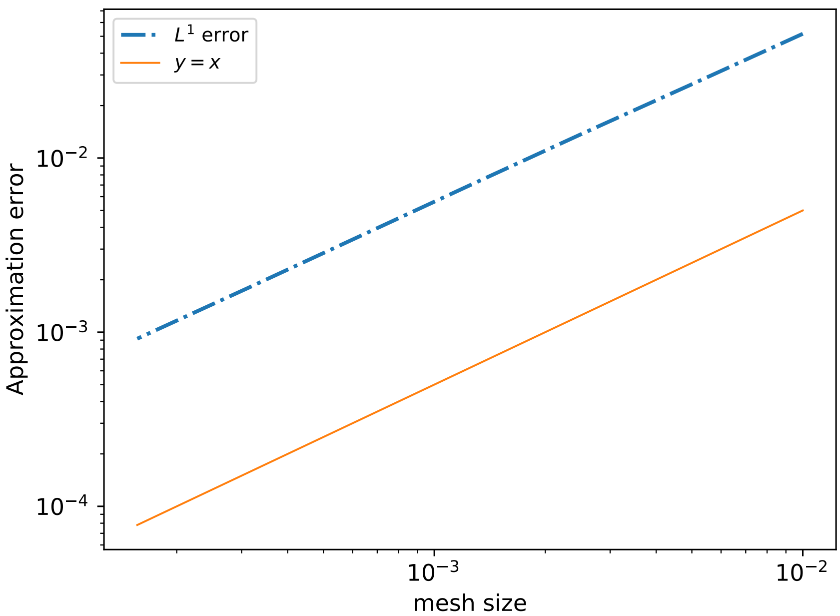


FIGURE 6.2. $L^1$ norm of the error at T=0.05s and CFL= $\dfrac{1}{10}$ – upwind interpolation.

We can also see the behavior of the scheme if we use discontinuous initial data. This type of numerical tests is of interest, as the G-equation is used in more complex physical models to track front propagation, such as the flame front propagation during a deflagration phenomenon. The front indicator is then often discontinuous.

We consider the following initial data:

$$G_0(x) = \left| \begin{array}{ll} 0 & \text{if } x \leq 0.5, \\ 1 & \text{otherwise.} \end{array} \right.$$

The result at time $T = 0.2s$ is given in figure 6.3, for the upwind scheme and the MUSCL scheme.

The MUSCL scheme brings less numerical diffusion, as expected. Normally one cannot define a viscosity solution for discontinuous initial data. However one expects the solution to be the same as the general viscosity solution given for BUC initial data (see (A.1) in the Appendix).

We know turn to computations in two dimensions.

## 6.2. **Two Dimensions**

### 6.2.1. *Unstructured grid*

The computational domain is $\Omega = [-\dfrac{1}{2}, \dfrac{1}{2}]^2$. The mesh consists in convex quadrilaterals. We give an example of the discretization in figure 6.4. These grids are built from a regular Cartesian grid for which a random displacement of length $\epsilon h$ is applied to each node where $h$ is the space step. We consider zero-flux boundary conditions. The initial data are given in the polar coordinates $(r, \theta)$:

$$G_0(r, \theta) = r \left(1 + \frac{1}{2} \cos(4\theta)\right).$$

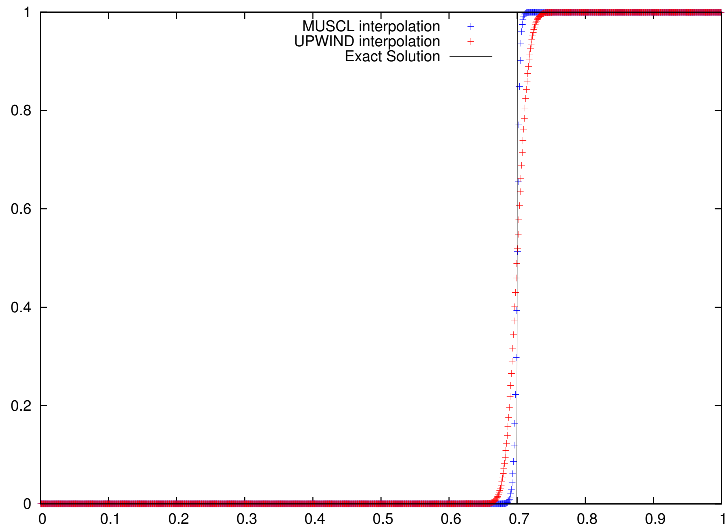


Figure 6.3. solution at $T = 0.05s$ and CFL$= \dfrac{1}{10}$ with $h = 10^{-3}$.

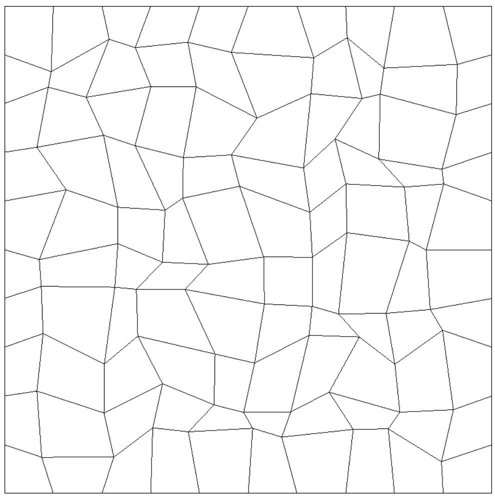

Figure 6.4. Example of a $10 \times 10$ unstructured grid.

Results obtained at different times are plotted on figure 6.5. The scheme used is the upwind version for unstructured meshes, with a space step equal to $h = \dfrac{1}{200}$ and a constant CFL number equal to $\frac{1}{10}$. Another possible test case is given by the following initial condition:

$$G_0(r, \theta) = |\sin(4\pi r)|. \tag{6.2}$$

This initial function is periodic and contains multiple local extrema. It allows to easily highlight the maximum principle verified by the discrete solution of the scheme. Results obtained with different meshes are displayed on figure 6.6. The scheme used is the upwind version for unstructured meshes,

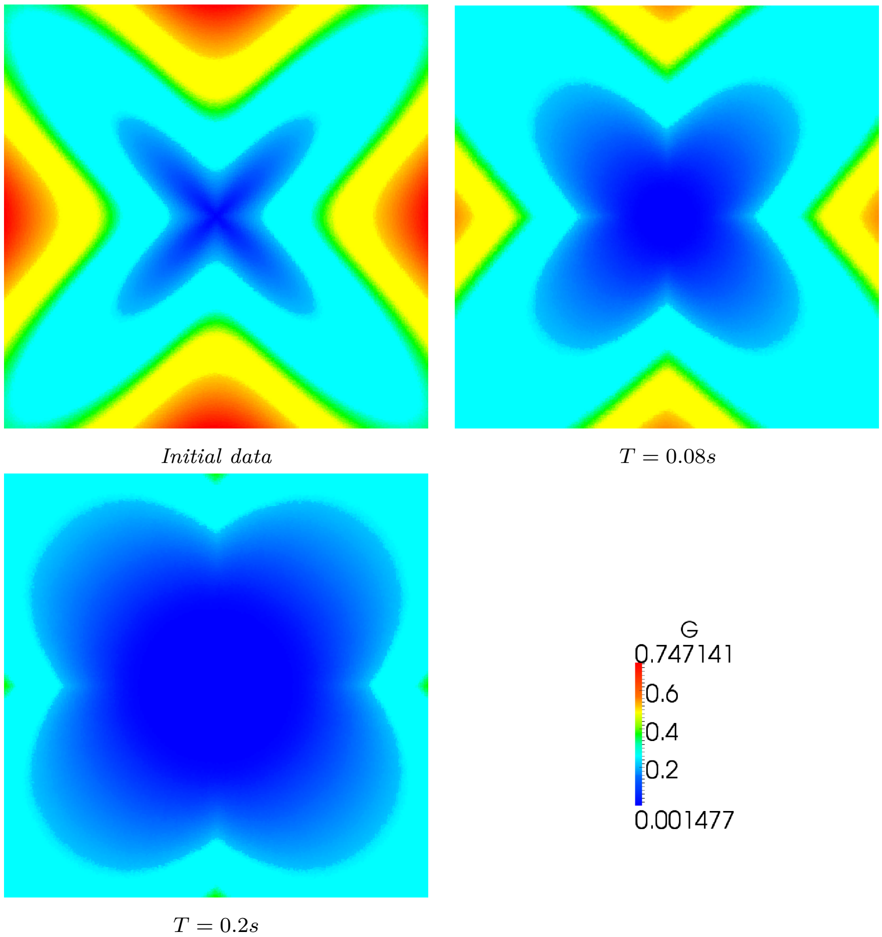


Figure 6.5. $G$ at different times with the upwind scheme on an unstructured mesh – $h = \dfrac{1}{200}$ – $CFL = \dfrac{1}{10}$.

with a space step equal to $h = \dfrac{1}{400}$, a constant CFL number equal to $\frac{1}{10}$ and a final time equal to $T = 0.04s$.

Finally we plot some convergence results. Let $G_{\text{visc}}$ be the viscosity solution associated with the initial data (6.2). We take $G_{\text{visc}}(., T = 0.01s)$ as a new initial data. The final time is set to $T = 0.04s$. The results are given on figure 6.7, with a constant CFL number equal to $\frac{1}{10}$, using three different meshes : an unstructured mesh with a deformation ratio equal to $\epsilon = 0.1$, a triangular mesh which consists of a square grid where each square is cut in half following the same diagonal, and a rhomboidal mesh composed of parallelograms with a large angle equal to $\frac{2\pi}{3}$. All these meshes are derived from a $400 \times 400$ grid except for the triangular mesh where a $200 \times 200$ grid is used.

### 6.2.2. *Cartesian grids*

We use the same test to compare the convergence of the MUSCL scheme, the upwind scheme, and an upwind finite difference scheme described in [10] designed for the Hamilton-Jacobi equations. This scheme is derived from classical discretization for conservation laws. In order to properly observe a

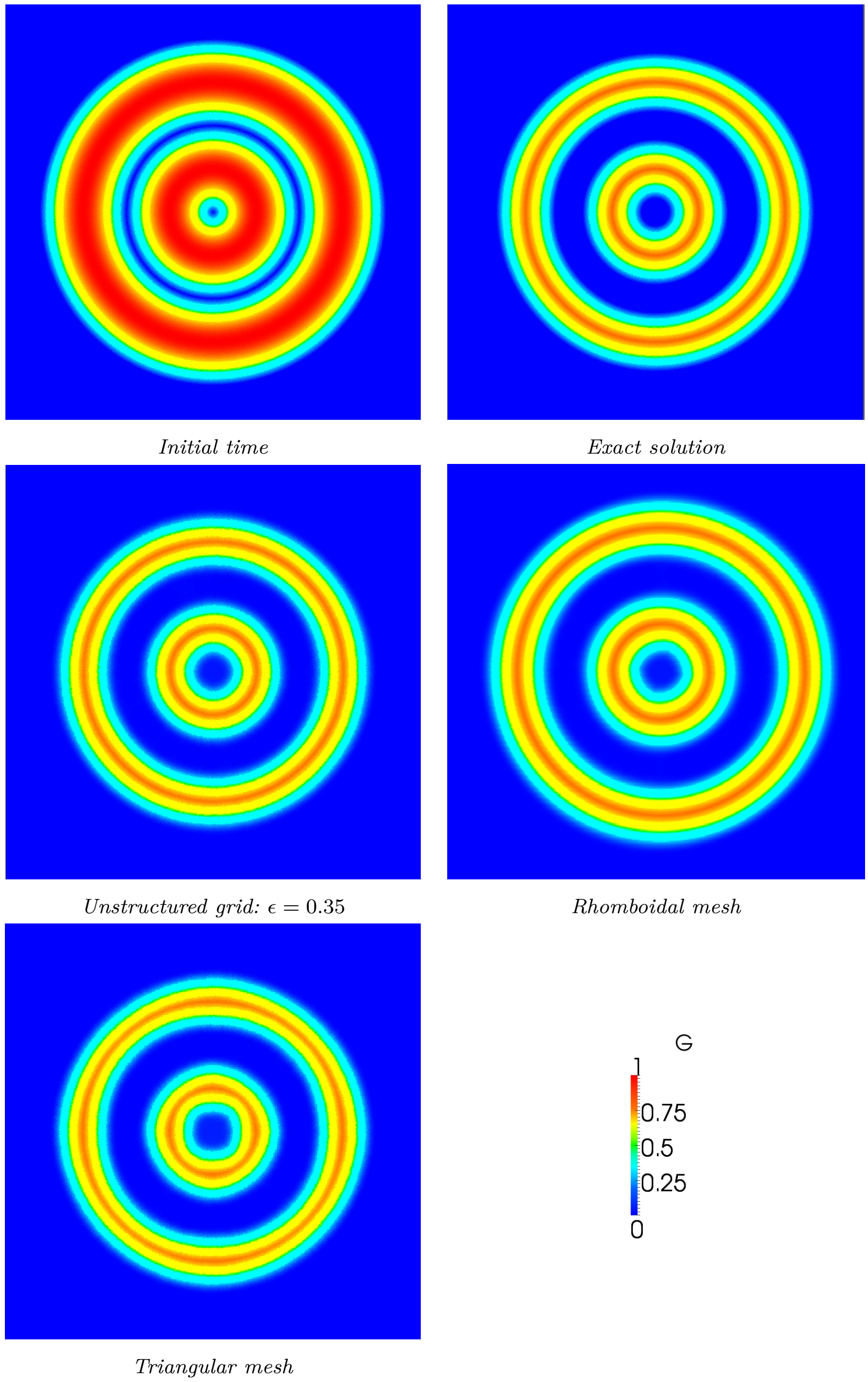


FIGURE 6.6. $G$ on different meshes – $T = 0.04s$ – $h = \dfrac{1}{400}$ – $CFL = \dfrac{1}{10}$.

difference in the convergence rate we use a Runge-Kutta time discretization of order two. Results are presented on figure 6.8.

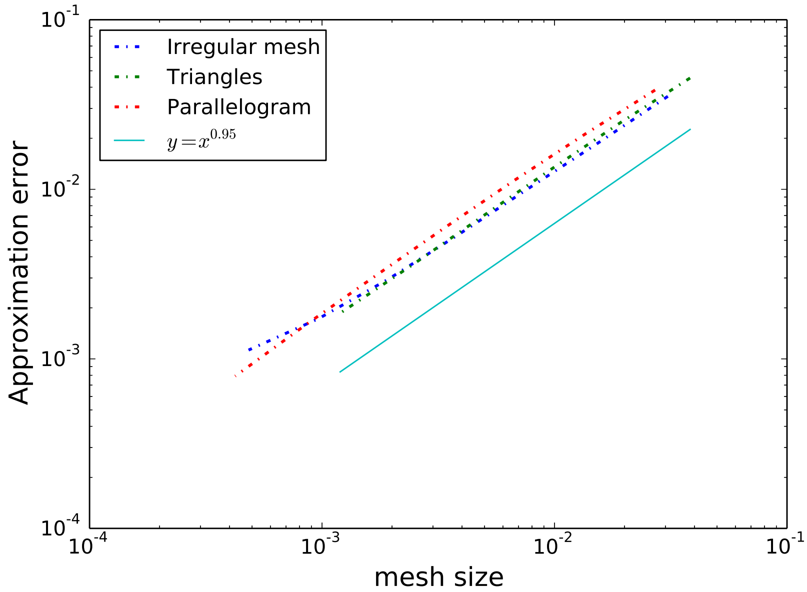


Figure 6.7. $L^1$ norm of the error at T=0.05s and CFL= $\dfrac{1}{10}$ – upwind interpolation.

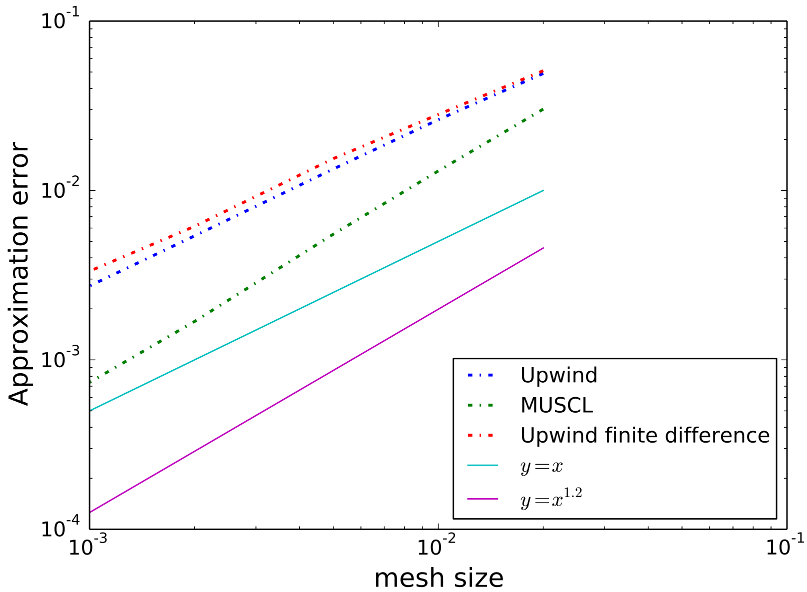


Figure 6.8. $L^1$ norm of the error at $T = 0.05s$ and CFL= $\dfrac{1}{10}$.

To conclude, we introduce a test case with a convective velocity $\boldsymbol{u}$ different from zero. Let the computational domain be $\Omega = (0, 1)^2$. Zero-flux boundary conditions are prescribed on the boundary.

We consider the following initial data

$$G_0(x) = \begin{vmatrix} 0 & \text{if } \|\boldsymbol{x} - (0.25, 0.8)\| \leq 0.15, \\ 1 & \text{otherwise.} \end{vmatrix}$$

The front propagation velocity is equal to $u_f = 0.8$ and the convective velocity corresponds to a vortex centered around $(0, 0)$ with a constant angular speed equal to $2\pi$, namely

$$\boldsymbol{u} = 2\pi r \boldsymbol{e}_\theta,$$

in polar coordinates.

The upwind scheme is used on a $400 \times 400$ Cartesian grid with a CFL number equal to $\frac{1}{20}$. Results are plotted on figure 6.9.

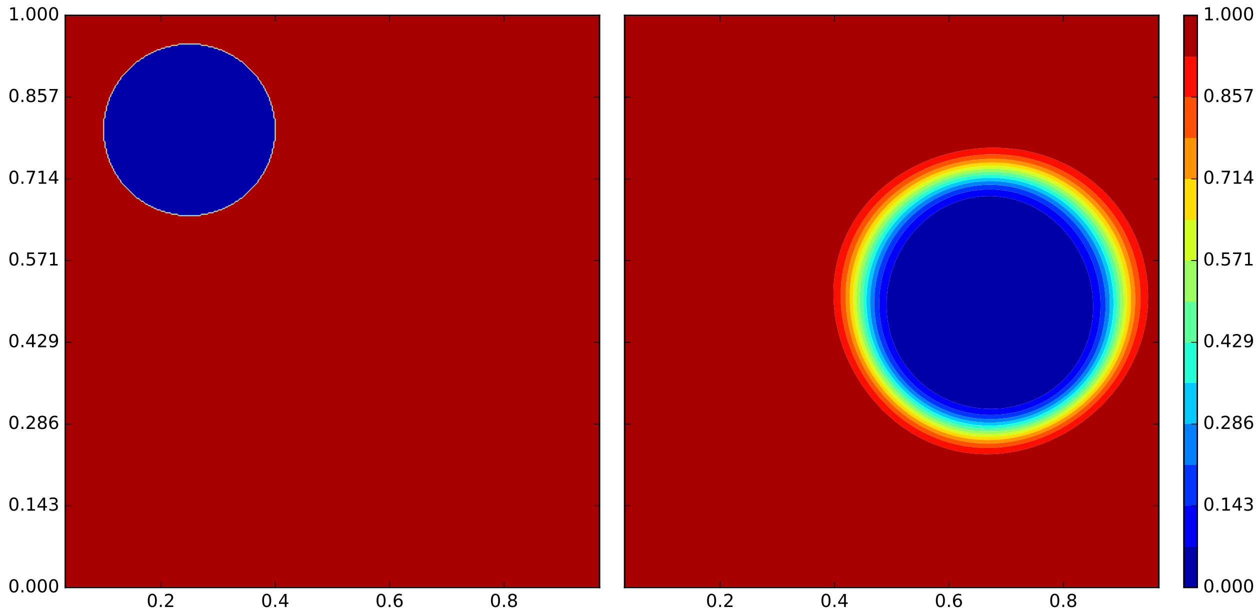


Figure 6.9. $G$ at $T = 0s$ (left) – $T = 0.1s$ (right) with a CFL$= \dfrac{1}{20}$.

Numerical simulations performed in this section are in good agreement with the properties verified by the scheme.

## Appendix A. Viscosity solutions of the eikonal equation

It is possible to compute the viscosity solution of (1.6) for every $G_0 \in BUC(\mathbb{R}^d)$. It is defined on $\mathbb{R}^d \times (0, +\infty)$ by:

$$G(\boldsymbol{x}, t) = \inf_{|\boldsymbol{x}-\boldsymbol{y}| \leq t} G_0(\boldsymbol{y}). \tag{A.1}$$

The proof of this result can be found in [3], and it is based on the following lemma:

**Lemma A.1.** *Let us set*

$$S(t)G(\boldsymbol{x}) = \inf_{|\boldsymbol{x}-\boldsymbol{y}| \leq t} G(\boldsymbol{y}).$$

*Then $S$ is a monotonous semigroup on $C(\mathbb{R}^d)$.*

**Proof.** The proof is rather simple as

$$S(t)\circ S(s)G(\boldsymbol{x}) = \inf_{|\boldsymbol{x}-\boldsymbol{y}|\le t}\left(\inf_{|\boldsymbol{z}-\boldsymbol{y}|\le s} G(\boldsymbol{z})\right).$$

This computation is equivalent to seek the infimum in the set

$$\{\boldsymbol{z} \text{ such that } \exists \boldsymbol{y} \text{ such that } |\boldsymbol{x}-\boldsymbol{y}|\le t \text{ and } |\boldsymbol{z}-\boldsymbol{y}|\le s\}.$$

Now, this set is equal to the set

$$\{\boldsymbol{z} \text{ such that } |\boldsymbol{x}-\boldsymbol{z}|\le t+s\},$$

so the infimum are equal and $S(t+s) = S(t)\circ S(s)$. Now consider $G_1$ and $G_2$ two functions of $C(\mathbb{R}^d)$ such that $G_1 \le G_2$ and let $t > 0$. Thanks to the continuity of $G_2$, $\exists \boldsymbol{y}_{\boldsymbol{x},t} \in B(\boldsymbol{x}, t)$ (the ball of center $\boldsymbol{x}$ and radius $t$) such that $S(t)G_2(x) = G_2(\boldsymbol{y}_{\boldsymbol{x},t})$. Consequently $G_2(\boldsymbol{y}_{\boldsymbol{x},t}) \ge G_1(\boldsymbol{y}_{\boldsymbol{x},t}) \ge S(t)G_1(x)$, which concludes the proof. ∎

Now let $\phi \in C^1(\mathbb{R}^d \times (0,+\infty))$ and suppose that $(\boldsymbol{x}, t)$ is a local maximum of $G-\phi$. Thanks to the semigroup property of $S$ we get that:

$$G(\boldsymbol{x},t) = S(t)G_0(\boldsymbol{x}) = S(h)S(t-h)G_0(\boldsymbol{x}) = S(h)G(\boldsymbol{x},t-h).$$

Therefore, for all $0 < h < t$, we have

$$G(\boldsymbol{x},t) = \inf_{|\boldsymbol{x}-\boldsymbol{y}|\le h} G(\boldsymbol{y},t-h). \tag{A.2}$$

$(\boldsymbol{x}, t)$ being a local maximum of $G-\phi$, we have, if $h$ is sufficiently small, and $|\boldsymbol{x}-\boldsymbol{y}| \le h$:

$$G(\boldsymbol{y},t-h) - \phi(\boldsymbol{y},t-h) \le G(\boldsymbol{x},t) - \phi(\boldsymbol{x},t),$$

which is equivalent to

$$G(\boldsymbol{y},t-h) \le G(\boldsymbol{x},t) - \phi(\boldsymbol{x},t) + \phi(\boldsymbol{y},t-h).$$

Injecting this in (A.2) leads to

$$\phi(\boldsymbol{x},t) \le \inf_{|\boldsymbol{x}-\boldsymbol{y}|\le h} \phi(\boldsymbol{y},t-h).$$

A first order Taylor expansion at the point $(\boldsymbol{x}, t)$ leads to

$$0 \le \inf_{|\boldsymbol{x}-\boldsymbol{y}|\le h}\left[-\partial_t\phi(\boldsymbol{x},t) + \boldsymbol{\nabla}\phi(\boldsymbol{x},t)\cdot\frac{\boldsymbol{y}-\boldsymbol{x}}{h} + o(1)\right].$$

Using that fact that $-\inf(-X) = \sup(X)$, we have

$$\partial_t\phi(\boldsymbol{x},t) + \sup_{|\boldsymbol{x}-\boldsymbol{y}|\le h} \boldsymbol{\nabla}\phi(\boldsymbol{x},t)\cdot\frac{\boldsymbol{x}-\boldsymbol{y}}{h} + o(1) \le 0.$$

Thanks to the Cauchy-Schwarz inequality:

$$|\boldsymbol{\nabla}\phi(\boldsymbol{x},t)\cdot\frac{\boldsymbol{x}-\boldsymbol{y}}{h}| \le |\boldsymbol{\nabla}\phi(\boldsymbol{x},t)|.$$

By taking $\boldsymbol{y} = \boldsymbol{x} - \dfrac{\boldsymbol{\nabla}\phi(\boldsymbol{x},t)}{|\boldsymbol{\nabla}\phi(\boldsymbol{x},t)|}h$ we see that the previous upper-bound is reached. Therefore,

$$\partial_t\phi(\boldsymbol{x},t) + |\boldsymbol{\nabla}\phi(\boldsymbol{x},t)| + o(1) \le 0,$$

and passing to the limit when $h \to 0$ leads to the desired result.

## Appendix B. Practical formulation of the scheme on Cartesian grids

The purpose of this section is to give a finite difference formulation of the scheme to be able to compare it easily with classical methods for the Hamilton-Jacobi equations. Without loss of generality we focus on the 2D scheme. Consider a discretization of the domain $\Omega$ in an $L \times L$ grid of constant space step in each direction $\Delta x = \Delta y = h$. Each cell is numbered by the doublet $(i,j) \in [\![0, L-1]\!]^2$. Then the upwind scheme reads

$$\eth_t G^n_{i,j} + \frac{1}{h}\Big((Fx^+)^n_{i+1/2,j} - (Fx^-)^n_{i-1/2,j} + (Fy^+)^n_{i,j+1/2} - (Fy^-)^n_{i,j-1/2}\Big) = 0,$$

with

$$(Fx^+)^n_{i+1/2,j} = \frac{|G^n_{i+1,j} - G^n_{i,j}|}{\sqrt{(G^n_{i+1,j} - G^n_{i,j})^2 + |\nabla^\perp_x G^n_{i+1,j}|^2}}\Theta(G^n_{i+1,j} - G^n_{i,j}),$$

$$(Fx^-)^n_{i+1/2,j} = \frac{|G^n_{i+1,j} - G^n_{i,j}|}{\sqrt{(G^n_{i+1,j} - G^n_{i,j})^2 + |\nabla^\perp_x G^n_{i,j}|^2}}\left\{1 - \Theta(G^n_{i+1,j} - G^n_{i,j})\right\},$$

$$(Fy^+)^n_{i,j+1/2} = \frac{|G^n_{i,j+1} - G^n_{i,j}|}{\sqrt{(G^n_{i,j+1} - G^n_{i,j})^2 + |\nabla^\perp_y G^n_{i,j+1}|^2}}\Theta(G^n_{i,j+1} - G^n_{i,j}),$$

$$(Fy^-)^n_{i,j+1/2} = \frac{|G^n_{i,j+1} - G^n_{i,j}|}{\sqrt{(G^n_{i,j+1} - G^n_{i,j})^2 + |\nabla^\perp_y G^n_{i,j}|^2}}\left\{1 - \Theta(G^n_{i,j+1} - G^n_{i,j})\right\},$$

where $\Theta(x) = \dfrac{x - |x|}{2x}$ for $x \neq 0$, $\Theta(0) = 0$, and

$$\nabla^\perp_x G^n_{i,j} = (G^n_{i,j+1} - G^n_{i,j})^+ - \frac{1}{2}\Big(1 - \operatorname{sgn}(G^n_{i,j+1} - G^n_{i,j})\Big)(G^n_{i,j} - G^n_{i,j-1})^-,$$

$$\nabla^\perp_y G^n_{i,j} = (G^n_{i+1,j} - G^n_{i,j})^+ - \frac{1}{2}\Big(1 - \operatorname{sgn}(G^n_{i+1,j} - G^n_{i,j})\Big)(G^n_{i,j} - G^n_{i-1,j})^-.$$

## References


[1] R. Abgrall. Numerical discretization of the first-order Hamilton-Jacobi equation on triangular meshes. *Comm. Pure Appl. Math.*, 49(12):1339–1373, 1996.

[2] S. Augoula and R. Abgrall. High order numerical discretization for Hamilton-Jacobi equations on triangular meshes. *J. Sci. Comput.*, 15(2):197–229, 2000.

[3] G. Barles. *Solutions de viscosité des équations de Hamilton-Jacobi*, volume 17 of *Mathématiques & Applications (Berlin) [Mathematics & Applications]*. Springer-Verlag, Paris, 1994.

[4] G. Barles and P. E. Souganidis. Convergence of approximation schemes for fully nonlinear second order equations. *Asymptotic Anal.*, 4(3):271–283, 1991.

[5] T. J. Barth and J. A. Sethian. Numerical schemes for the Hamilton-Jacobi and level set equations on triangulated domains. *J. Comput. Phys.*, 145(1):1–40, 1998.

[6] S. Bryson and D. Levy. High-order central WENO schemes for multidimensional Hamilton-Jacobi equations. *SIAM J. Numer. Anal.*, 41(4):1339–1369 (electronic), 2003.

[7] C. Chalons, M. Girardin, and S. Kokh. An all-regime lagrange-projection like scheme for 2d homogeneous models for two-phase flows on unstructured meshes. *Journal of Computational Physics*, 335:885 – 904, 2017.

[8] P. G. Ciarlet. Basic error estimates for elliptic problems. In P. Ciarlet and J.L. Lions, editors, *Handbook of Numerical Analysis, Volume II*, pages 17–351. North Holland, 1991.

[9] M. G. Crandall and P.-L. Lions. Viscosity solutions of Hamilton-Jacobi equations. *Trans. Amer. Math. Soc.*, 277(1):1–42, 1983.

[10] M. G. Crandall and P.-L. Lions. Two approximations of solutions of Hamilton-Jacobi equations. *Math. Comp.*, 43(167):1–19, 1984.

[11] C. M. Dafermos. *Hyperbolic conservation laws in continuum physics.* Berlin: Springer, 4th edition, 2016.

[12] S. Dellacherie, J. Jung, P. Omnes, and P.-A. Raviart. Construction of modified Godunov-type schemes accurate at any Mach number for the compressible Euler system. *Math. Models Methods Appl. Sci.*, 26(13):2525–2615, 2016.

[13] R. Eymard, T. Gallouët, and R. Herbin. Discretization of heterogeneous and anisotropic diffusion problems on general nonconforming meshes SUSHI: a scheme using stabilization and hybrid interfaces. *IMA J. Numer. Anal.*, 30(4):1009–1043, 2010.

[14] D. Grapsas. *Schémas à mailles décalés pour des modèles d'écoulements compressible réactifs.* PhD thesis, Université Aix-Marseille, 2018.

[15] D. Grapsas, R. Herbin, W. Kheriji, and J.-C. Latché. An unconditionally stable staggered pressure correction scheme for the compressible Navier-Stokes equations. *SMAI Journal of Computational Mathematics*, 2:51–97, 2016.

[16] F.H. Harlow and A.A. Amsden. Numerical calculation of almost incompressible flow. *Journal of Computational Physics*, 3:80–93, 1968.

[17] F.H. Harlow and A.A. Amsden. A numerical fluid dynamics calculation method for all flow speeds. *Journal of Computational Physics*, 8:197–213, 1971.

[18] F.H. Harlow and J.E. Welsh. Numerical calculation of time-dependent viscous incompressible flow of fluid with free surface. *Physics of Fluids*, 8:2182–2189, 1965.

[19] R. Herbin, W. Kheriji, and J.-C. Latché. Staggered schemes for all speed flows. *ESAIM, Proc.*, 35:122–150, 2012.

[20] R. Herbin, W. Kheriji, and J.-C. Latché. On some implicit and semi-implicit staggered schemes for the shallow water and Euler equations. *ESAIM Math. Model. Numer. Anal.*, 48(6):1807–1857, 2014.

[21] R. Herbin, J.-C. Latché, and T. T. Nguyen. Explicit staggered schemes for the compressible Euler equations. In *Applied mathematics in Savoie—AMIS 2012: Multiphase flow in industrial and environmental engineering*, volume 40 of *ESAIM Proc.*, pages 83–102. EDP Sci., Les Ulis, 2013.

[22] IRSN. $P^2$REMICS: Computational fluid dynamics software for the simulation of dispersion and explosion. `https://gforge.irsn.fr/gf/project/p2remics`.

[23] G. Kossioris, Ch. Makridakis, and P. E. Souganidis. Finite volume schemes for Hamilton-Jacobi equations. *Numer. Math.*, 83(3):427–442, 1999.

[24] P.-L. Lions. *Generalized solutions of Hamilton-Jacobi equations*, volume 69 of *Research Notes in Mathematics.* Pitman (Advanced Publishing Program), Boston, Mass.-London, 1982.

[25] S. Osher and J. A. Sethian. Fronts propagating with curvature-dependent speed: algorithms based on Hamilton-Jacobi formulations. *J. Comput. Phys.*, 79(1):12–49, 1988.

[26] S. Osher and C.-W. Shu. High-order essentially nonoscillatory schemes for Hamilton-Jacobi equations. *SIAM J. Numer. Anal.*, 28(4):907–922, 1991.

[27] Y. Penel, S. Dellacherie, and B. Després. Coupling strategies for compressible-low Mach number flows. *Math. Models Methods Appl. Sci.*, 25(6):1045–1089, 2015.

[28] L. Piar, F. Babik, R. Herbin, and J.-C. Latché. A formally second-order cell centred scheme for convection-diffusion equations on general grids. *Internat. J. Numer. Methods Fluids*, 71(7):873–890, 2013.

[29] S. Serna and J. Qian. Fifth-order weighted power-ENO schemes for Hamilton-Jacobi equations. *J. Sci. Comput.*, 29(1):57–81, 2006.

[30] J. A. Sethian and A. Vladimirsky. Fast methods for the eikonal and related Hamilton-Jacobi equations on unstructured meshes. *Proc. Natl. Acad. Sci. USA*, 97(11):5699–5703, 2000.

[31] P. E. Souganidis. Approximation schemes for viscosity solutions of Hamilton-Jacobi equations. *J. Differential Equations*, 59(1):1–43, 1985.

[32] J. Yan and S. Osher. A local discontinuous Galerkin method for directly solving Hamilton-Jacobi equations. *J. Comput. Phys.*, 230(1):232–244, 2011.